Powder Technology 338 (2018) 7–16

Contents lists available at ScienceDirect

Powder Technology

journal homepage: www.elsevier.com/locate/powtec

Compressive deformation of liquid marbles

Rane Y., Foster E., Moradiafrapoli M., Marston J.O. *

Department of Chemical Engineering, Texas Tech University, Lubbock, TX 79409, United States

ARTICLE INFO

Article history:
Received 27 November 2017
Received in revised form 21 March 2018
Accepted 24 May 2018
Available online 24 June 2018

Keywords:
Liquid marbles
Armored interface
Rupture
Hysteresis

ABSTRACT

Millimetric liquid droplets coated with particles, known as "liquid marbles", exhibit some curious physical properties such as extended lifetime with regards to evaporation, low-friction when in contact with other surfaces and non-coalescence with other liquids. The formation dynamics have been well-characterized as well as thermal properties, however, their mechanical properties have not. Here, we investigate the response of liquid marbles to compressive deformation between two plates. Above a compressive strain of approximately 40–50%, cracks appear in the particle coating and the liquid can wet the surface of the plates, i.e. the marble ruptures. However, more strikingly, we find that even for relatively small compressive strain (without rupturing), the marbles often undergo an irreversible deformation - that is they do not regain their original shape. We quantify this shape 'hysteresis' across a range of particle sizes and liquids, showing that it correlates primarily with compressive strain, but also particle type and underlying fluid. Furthermore, we analyse the compressed marble shapes upon approach to rupture in the context of previous analytical approximations, showing that the recent theory of Whyman & Bormashenko (2015) provides a good description of crushed marble shapes.

1. Introduction

Liquid marbles are millimetric droplets coated with particles [1–6]. In order to form a liquid marble, the particles must remain at the surface and most studies therefore use hydrophobic particles, although it is possible to use hydrophilic particles [7]. This shell of particles inhibits the liquid inside from making physical contact with surfaces outside, be they solid or liquid. As such, a liquid marble placed on a solid surface exhibits a non-wetting state, shown in Fig. 1. Only a slight deformation is observed at the base due to gravity [2, 3] since the marble diameter, D, is comparable to the capillary length $l_c = \sqrt{\sigma/(\rho g)}$, where σ is the liquid surface tension, ρ is the liquid density, and g is the acceleration due to gravity.

The formation of liquid marbles is an interesting phenomenon which has been studied extensively (e.g. [8–14]), eluding to some critical conditions in terms of liquid properties, and droplet to particle diameter ratio, D/d_p.

Some of the proposed applications of liquid marbles such as sensors, micro-reactors, transporters etc. [15–22], rely on the mobility of the marble, which in turn appears to depend on the packing structure of particles at the surface. If the surface coverage is too low, then wetting may occur and destroy the integrity of the marble. However, when the packing becomes too dense and all the liquid free-surface disappears, it was shown ([12–14, 23–25]) that liquid marbles undergo an irreversible deformation to a jammed interface, where non-spherical marbles form. This is clearly an undesirable state in the context of mobility. Therefore, understanding their robustness and elasticity is paramount, yet to date, only a few studies have elucidated to mechanical properties. In particular, we note the works of [26–28] where the response to gradual compression was measured, resulting in both forces and surface areas as functions of compression ratio (versus original shape). They found that the marbles could withstand a compression of up to approximately 30%. However, in each of these studies only a single combination (liquid-particle) was studied. Bormashenko and coworkers (e.g. [29–31]) have also perfomed studies on the elasticity of liquid marbles, where in particular, a simple model for the shape deformation could account for the observations of elasticity in [27, 28].

Here, we report on experiments of compressive deformation of liquid marbles, similar to [27, 28], but for a wide range of liquids and particle sizes. We not only measure the critical compression ratio at which marbles rupture, but we also perform compress-release experiments and observe that even a modest compression can result in irreversible deformation. Furthermore, the simple model of [30] for the shape deformation is quantitatively tested. Whilst the rupture appears to be independent of particle characteristics and liquid, the hysteresis is found to depend on the compressive strain, particle size and underlying liquid.

2. Materials and methods

Liquid marbles are prepared by allowing a droplet of water to gently contact a bed of hydrophobic glass beads. The droplet is then manually rolled across the surface until a complete coating is achieved and subsequently placed on a horizontal microscope slide. A top plate is placed

* Corresponding author.
E-mail address: jeremy.marston@ttu.edu (J.O. Marston).

https://doi.org/10.1016/j.powtec.2018.05.058
0032-5910/

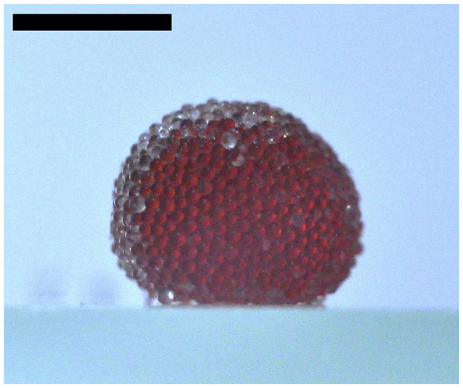

Fig. 1. A liquid marble at rest on a microscope slide. The marble is approximately 3 mm in diameter and the particles have a mean diameter of 178 μm. The scale bar is 2 mm long. Red food dye has been added for visualization purposes.

above the marble and then gradually lowered using a motorized translation stage (MTS50-Z8, Thorlabs Inc.) at a maximum speed $dz/dt = 1$ mm/s. The compression ratio, or vertical strain, is defined as $\epsilon_z = \Delta z/z_0$, whilst the elongation ratio, or horizontal strain, is defined as $\epsilon_x = (D - D_0)/D_0$, shown graphically in Fig. 2.

As depicted in Fig. 2, we performed two types of experiments: In the first experiment, the compression continues until the marble ruptures and the liquid wets one of the plates (Fig. 2(a)). In the second experiment, the compression was halted before rupture in order to assess the ability of the marble to regain its initial shape (Fig. 2(b)). In these compress-release cases, we characterized the deformation by comparing the initial and final shapes, i.e. $z_f - z_0$ and $D_f - D_0$. The process was captured by either high-speed video (Phantom Miro 310, Vision Research Inc.) or regular video (Nikon D90) with high-magnification to render effective pixel sizes of approximately 4.2 μm/px. The marble shapes are digitally extracted using a similar MatLab routine to that of [12], giving dimensions accurate to within ±4 px (2 px at each edge).

The particles comprised a range of glass beads and PTFE powders. The PTFE powder is naturally hydrophobic, whilst the glass beads were hydrophobized using the technique outlined in previous publications [12, 14, 23, 33]. The particle size distributions were characterized

Table 1
Volume-based particle size characteristics. All values stated are in μm. GB = glass beads. PTFE = Polytetrafluoroethylene powder.

Particulate label	d_{10}	d_{50}	d_{90}
GB: <53 μm	20.4	33.9	48.9
GB: 100 μm	89.2	126	169.9
GB: 100–300 μm	169	227	309
PTFE: 1 μm	0.77	1.03	1.62
PTFE: 35 μm	12.88	22.4	33.9

by the cumulative volume-based fractions (d_{10}, d_{50}, d_{90}), measured using an API Aerosizer (TSI Inc.), given in Table 1 and Fig. 3. In addition, microscope images revealed that the glass beads were circular, with $C = 4\pi A/P^2 \geq 0.9$, whilst the PTFE powders were coarse.

A water droplet placed on a layer of these powders typically exhibits an apparent contact angle between 145° and 155°, whilst images of isolated particles at the drop interface exhibit contact angles of approximate 120° (e.g. [32, 33]). NaCl and glycerin droplets exhibited slightly higher contact angles of approximately 160° and 155° respectively, however the SDS solution exhibited contact angles of approximately 87-95° for glass beads, but 120-140° for PTFE.

In order to study the possible influence of fluid properties, we used pure water, glycerin, surfactant and salt solutions, as detailed in Table 2. redBased upon these physical properties and radii of $R_0 \approx$ 1–1.6 mm, we estimate the following dimensionless number ranges:

$$Ca = \frac{\mu dz/dt}{\sigma} = 1.4 \times 10^{-5} - 1.2 \times 10^{-4}, \qquad Bo = \frac{\rho g R_0^2}{\sigma} = 0.13 - 0.81$$

$$Oh = \frac{\mu}{\sqrt{\rho \sigma R_0}} = 0.0037 - 0.0023$$

which confirm that this process is not expected to be dominated by viscosity, but capillary forces.

In some cases, red food dye was added to the water for visualization purposes, but did not result in any measurable change in physical properties. We also note that the experiment was conducted within the timespan of one minute, redat a constant abmient temperature of 22 °C so that we do not expect appreciable effects of evaporation.

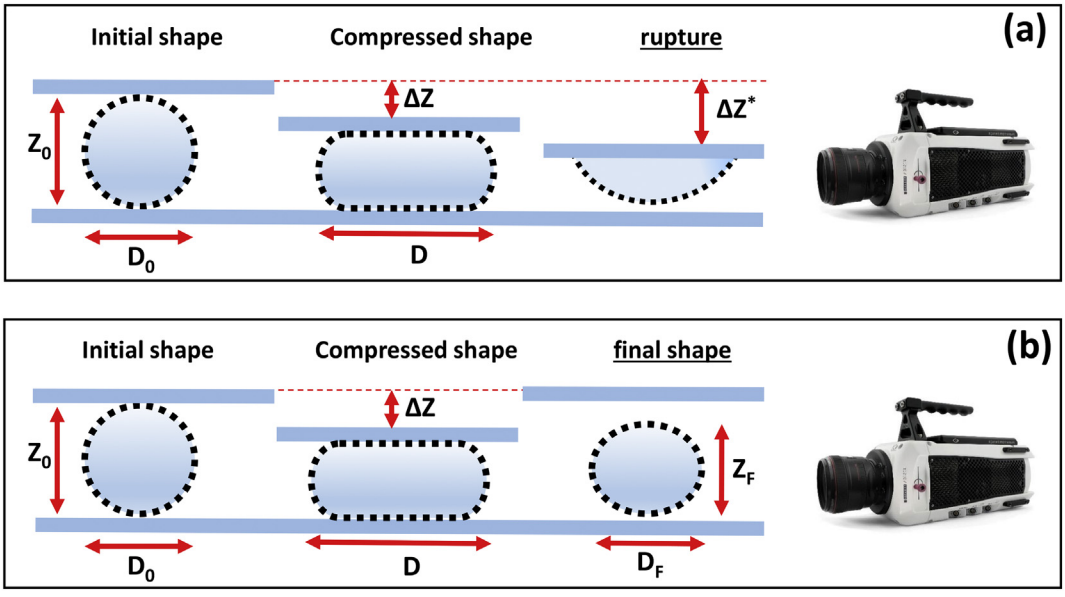

Fig. 2. Graphical definition of the measurements pertaining to the compression experiments. (a) Rupture experiment where the compressed shape upon approach to rupture is characterized by D and Δz and (b) compress-release experiment where the hysteresis is characterized by $(z_0 - z_f)/z_0$ vs. Δz.

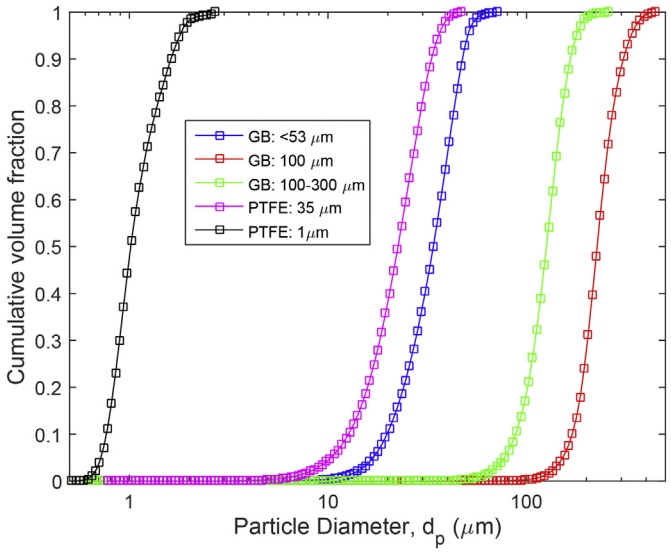

Fig. 3. Results from particle size analysis in the form of cumulative volume fraction versus particle diameter.

Table 2
Physical properties of the test liquids. Approximate concentrations are stated in $\%_{w/w}$.

Liquid	Density ρ (kg/m^3)	Viscosity μ (mPa.s)	Surface tension σ (mN/m)	Capillary length $\sqrt{\sigma/(\rho g)}$ (mm)
Water	1000	1	72	2.7
50% Glycerin	1130	8	67	2.5
0.5% SDS	~ 1000	1	31	1.75
29% NaCl	1187	1.4	80	2.6

3. Results

3.1. Qualitative overview

A typical sequence of events for a rupture experiment (Fig. 2(a)) is shown in Fig. 4. The marble sits on a glass plate and, due to the particulate shell separating the liquid from the plate, exhibits a non-wetting configuration. The top plate is gradually lowered and again, the particle shell on the upper portion of the marble prevents wetting. As the top plate is lowered further, the marble compresses in the vertical direction ($z < z_0$) and elongates in the horizontal direction ($D > D_0$) until cracks begin to appear in the surface (image 7, $\epsilon_z =$ 0.46). Further compression from this point leads to rupture, whereby the liquid wets the top plate, destroying the integrity of the marble. The compression ratio at this point is $\epsilon_z^* = 0.49$, i.e. rupture in this realization occurred when the marble was compressed to about half of the original height.

In Fig. 5(a), the liquid marble is compressed to $\epsilon_z = 0.33 < \epsilon_z^*$ but then released so that rupture does not occur. When the top plate is lifted high enough so that it no longer contacts the liquid marble, we digitally extract and overlay the initial and final shapes, shown by the blue and red outlines in Fig. 5(b). We observe that the marble has flattened - i.e. a decrease in height ($\epsilon_{z,\,final} = 0.09$) and increase in diameter ($\epsilon_{x,\,final} = 0.05$). In other words, the result of the compress-and-release procedure is an *irreversible* deformation of about 10% of the original height.

This observation is rather unexpected since the maximum compression in this case was $\epsilon_z = 0.33$ and previous reports [26, 27, 28] indicate that compression of a liquid marble with $\epsilon_z \sim 0.3$ should be reversible. To explore this observation further, we conducted a series of compress-and-release tests where the compression ratio was systematically increased from $\epsilon_z = 1$ down to $\epsilon_z = \epsilon_z^* \approx 0.5$. We also varied both the liquid and particle size to determine if the hysteresis was a generic feature of liquid marbles. We begin our quantitative analysis by seeking to describe the shape of compressed marbles, from which we can also calculate changes in surface area.

3.2. Description of deformed shape from volume conservation

With regards to the shape of the compressed marble, we note from Figs. 3 and 4 flat poles (top and bottom) and splayed edges, which we seek to quantitatively describe, The two analytical approximations in the literature for the deformed shapes of compressed liquid marbles can be found in Aussillous & Quere (2006) and Whyman & Bormashenko (2015). In the former, it is assumed that the marble with initial radius R_0 takes on an elliptical shape which, subject to compression ΔZ, has radius in the major axis, R and minor axis $R_0 - \frac{\Delta z}{2}$. Volume conservation then yields

$$R \approx \sqrt{\frac{R_0^3}{R_0 - \frac{\Delta z}{2}}} \tag{1}$$

In contrast, Whyman & Bormashenko (2015) consider two cases to derive the shape of compressed marbles. The first is for small

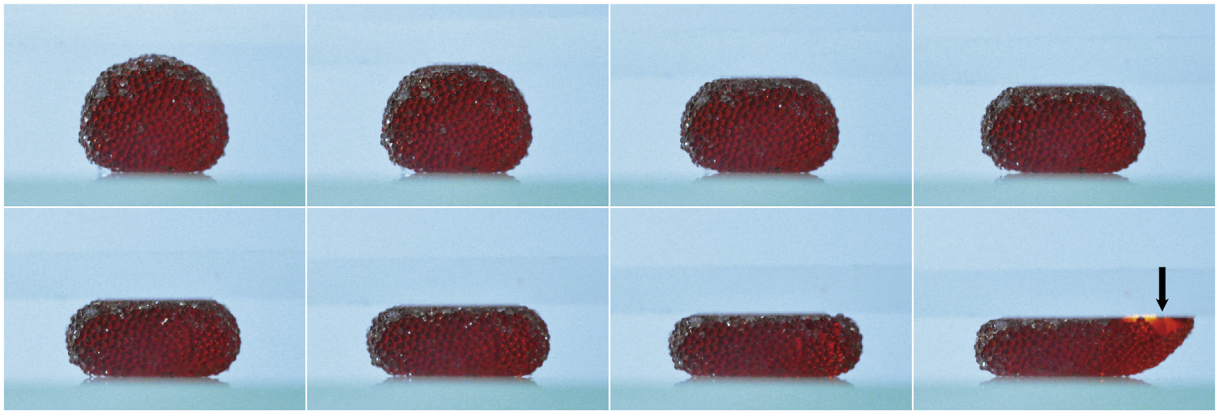

Fig. 4. Image sequence showing the step-wise compression of a water marble ($D_0 \approx 3.3$ mm, $d_p = 178$ μm). The compression ratios in frames 1–7 are $\epsilon_z = 0, 0.076, 0.186, 0.261, 0.341, 0.389, 0.464$, whilst the elongation ratios are $\epsilon_x = 0, 0.002, 0.067, 0.101, 0.21, 0.23$ and 0.29. The critical compression ratio $\epsilon_z^* = 0.494$, whereupon the marble ruptures and wets the upper surface, indicated by the arrow in the final image.

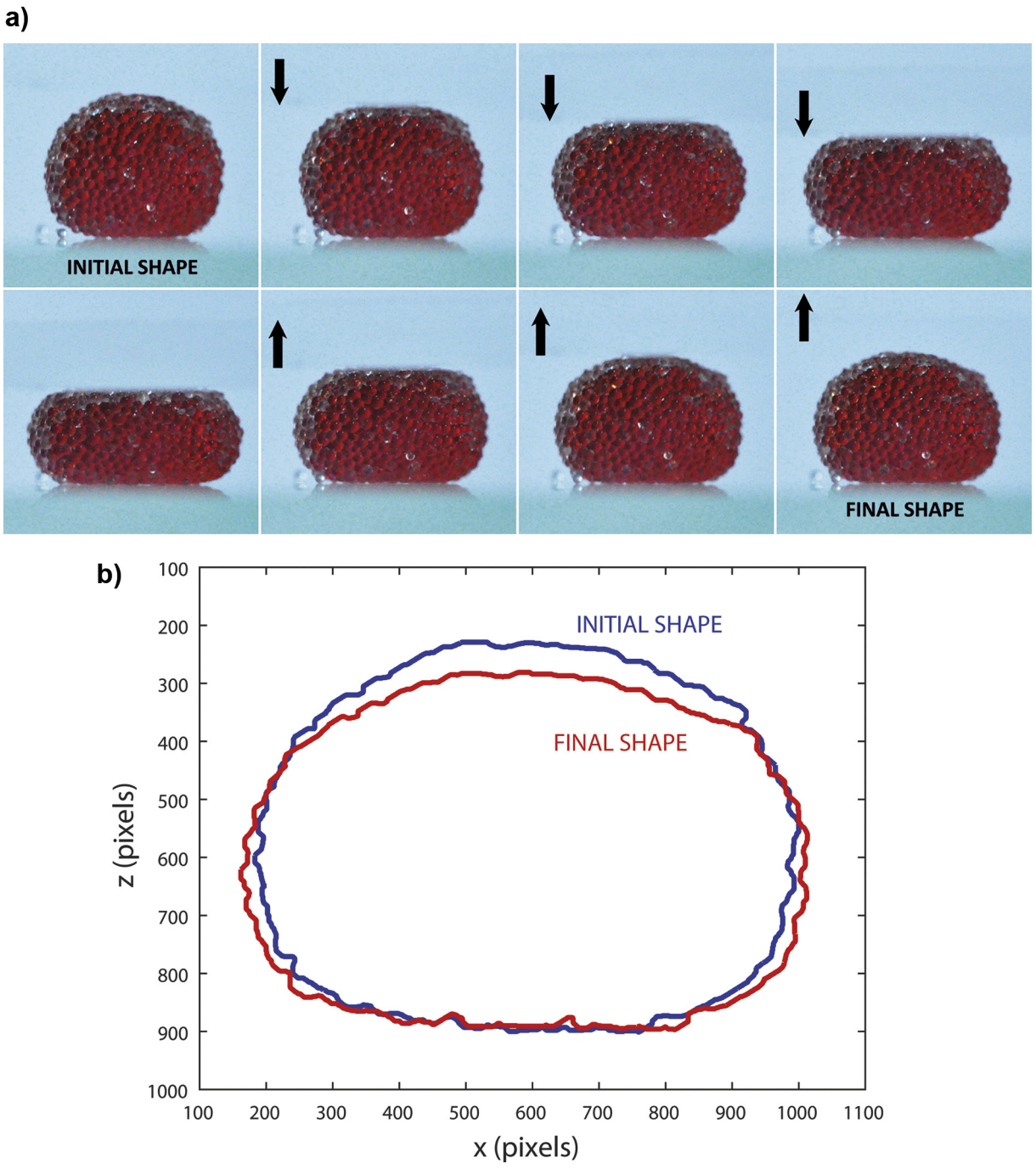

Fig. 5. (a) Image sequence showing the step-wise compression of a water marble ($D \approx 3.3$ mm, $d_p = 178$ μm). The marble is compressed to $\epsilon_z = 0.33$, then released (the arrows indicate the direction of motion of the top plate). The initial and final shapes are compared in (b), indicating a hysteresis of 9%.

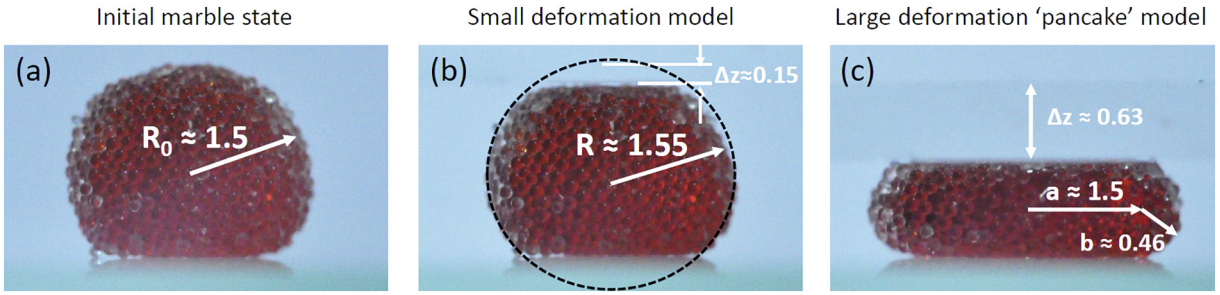

Fig. 6. Graphical definitions of parameters in the shape deformation models of [30] pertaining to Eqs. (2) and (3). The values of R, R_0, Δz, a, and b are stated in millimeters.

deformations, where the north and south poles of the marble become slightly flattened (see Fig. 6(b)), in which case the radius is

$$R \approx R_0 + \frac{(\Delta z)^2}{2R_0} - \frac{(\Delta z)^3}{6R_0^2} + O(\Delta z^5) \tag{2}$$

The second case is for highly compressed marbles, where the marble assumes a 'pancake' shape (see Fig. 5(c)). Flattened areas at the poles, given by the radius a, are now significant and the outer curved part has a much reduced radius of curvature, b. In this case, the expressions for these two radii are given in [30] as

$$a \approx R_0(a_1\epsilon_z + a_2\epsilon_z^2 + a_3\epsilon_z^3 + a_4\epsilon_z^4), \qquad b = R_0 - \Delta z \tag{3}$$

where the coefficients are $a_1 = 4/\pi$, $a_2 = \frac{4}{\pi}(1-\frac{8}{\pi^2})$, $a_3 \approx 0.2746$, $a_4 \approx 0.2168$. The total deformed radius for the pancake model is then $R = a + b$. Using the functional forms of the total radius given by Eqs. (1)–(3), the 'predicted' horizontal strain, $\epsilon_x = [R - R_0]/R_0$, can then be computed as a function of the horizontal strain, $\epsilon_z = \Delta z/z_0$, and the normalized functional form we seek is $\epsilon_x = \epsilon_x(\epsilon_z)$.

Taking these three approximations and plotting against our experimental data, we find that Eq. (1) fails to quantitatively describe our data, as shown in Fig. 7. However, the approximations from Eqs. (2) and (3) provide a reasonable description across the range of compressions we consider. We note that the comparison is very good at lower strains, $\epsilon_z \lesssim 25$ %, but that [2] slightly overestimates the elongation for higher strains, whilst [3] underestimates.

In particular, we find the crossover point for the two expressions in Eqs. (2) and (3) is $\epsilon_z \approx 0.19$. After the crossover point, the 'pancake' model of Eq. (3) predicts a lower elongation than that in Eq. (2). Given that the two approximations are for small and large deformations respectively, we could interpret this crossover point to represent the upper limit of applicability of Eq. (2) and the lower limit of Eq. (3), however, our data supports the use of Eq. (2). One should keep in mind that the mean diameters in most cases are slightly larger than the capillary lengths $l_c = \sqrt{\sigma/(\rho g)}$, which means that the marbles deform slightly under gravity before compression, which the two approximations do not account for. In fact, the pancake model is preferential for diameters greater than the capillary length. Therefore, the true marble shapes are likely to be confined between these two limiting cases, which is indeed the case.

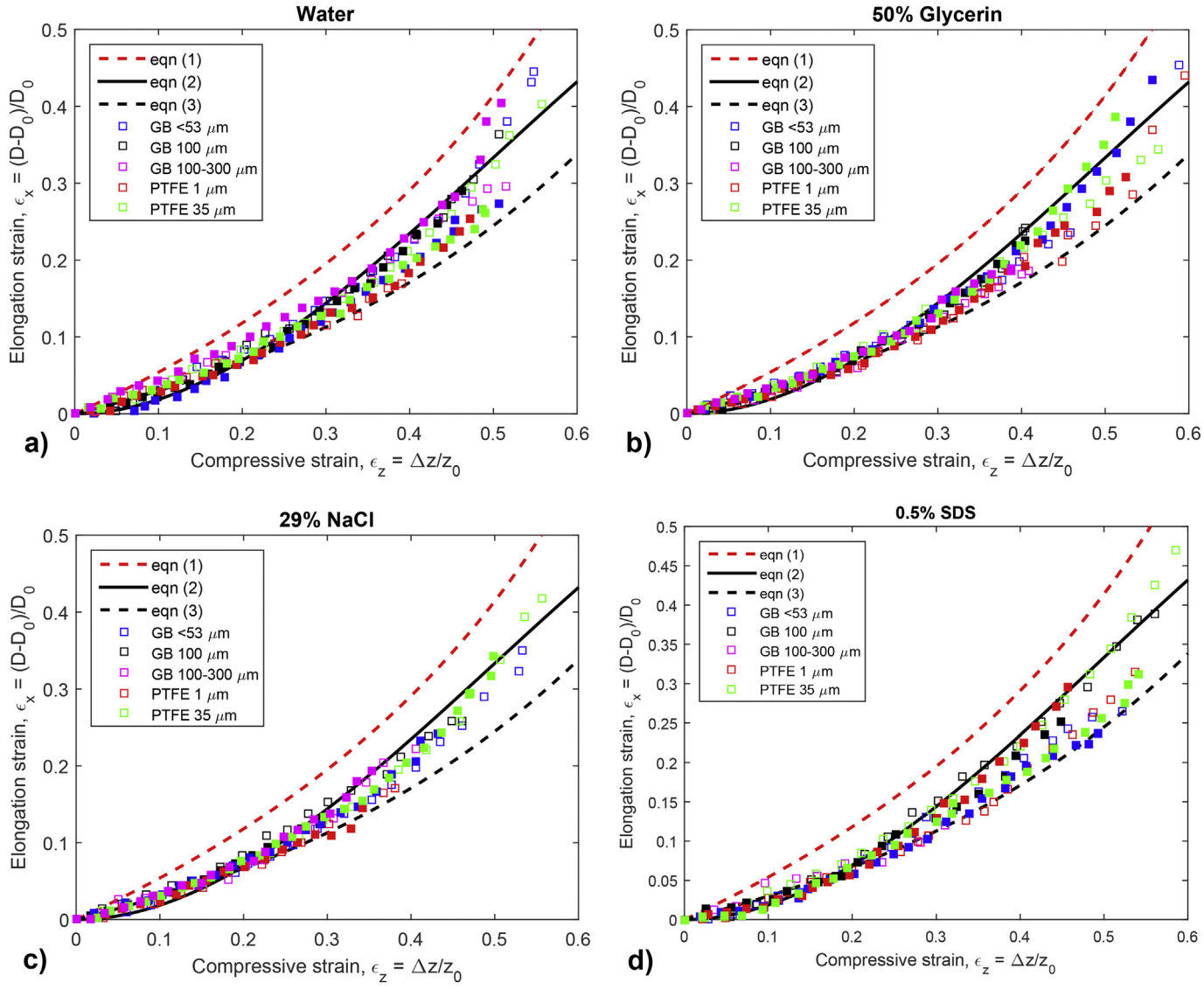

Fig. 7. Normalized shapes of liquid marbles for (a) Water, (b) 50% glycerin, (c) 29% NaCl, and (d) 0.5% SDS. The data points are the experimental data encompassing all particle sizes (see legend), whilst the dashed and solid lines represent the theoretical approximations from Eqs. (1), (2), and (3).

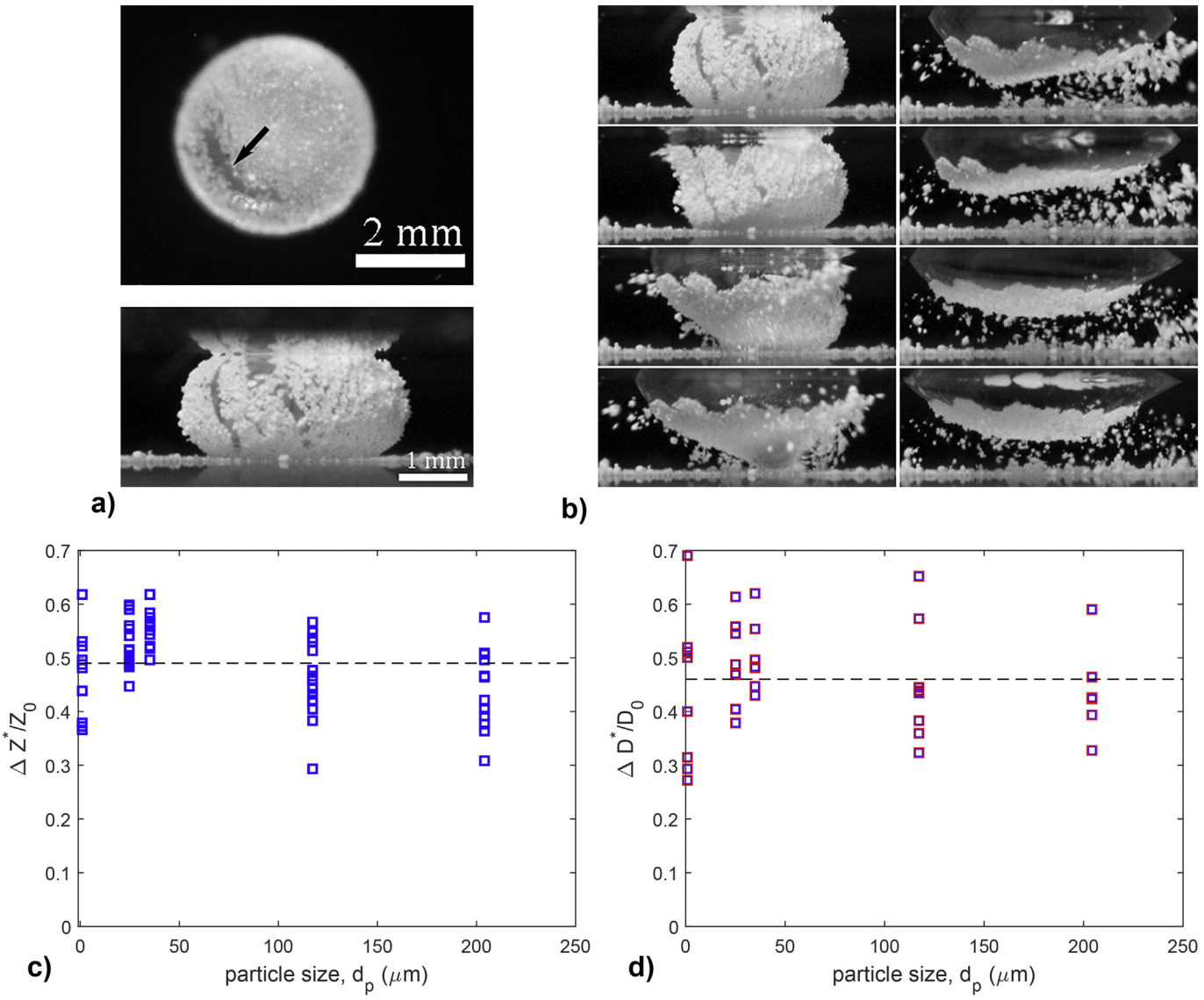

Fig. 8. (a): Top and side view images showing cracks just prior to rupture (top image: GB 100 μm, bottom image: PTFE 1 μ). (b): Rupture sequence showing the liquid wetting the upper plate. The time interval between frames is 2 ms. (c) and (d): Critical compressive and elongation strains, Δz^* and ΔD^*, versus particle diameter.

We note that the derivations for shapes of compressed marbles, unlike those for force, are independent of the effective surface tension and therefore one would expect the data from different liquids and different particles to collapse. This again is the case as our experimental data in Figs. 7(a)-(d) does not distinguish between the different combinations tested.

3.3. Rupture

The rupture of marbles was first experimentally studied by [3], in terms of the maximal diameter prior to rupture and then by [26] in terms of maximal force. Here, we seek to characterize both the shape (dimensions) and increase in surface area immediately prior to rupture. Fig. 8(a) shows images of marbles at this stage. What we notice is that the marbles have developed significant cracks in the particulate shell. It is this expsoure of free surface which allows liquid to contact the compression plates. The actual rupture process, when the liquid inside the marble finally wets one of the plates, can be quite violent (see Fig. 8(b)) when compared to a spherical droplet placed gently on a glass substrate (e.g. [34]) because the compressed shape is under higher Laplace pressure ($\Delta P \sim \frac{2\sigma}{Z_0-\Delta Z}$) [26] than an underformed droplet of the same volume ($\Delta P \sim \frac{2\sigma}{R_0}$).

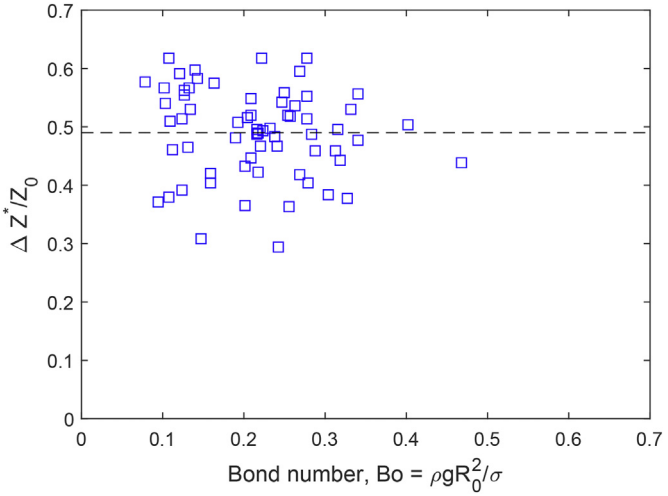

Fig. 9. Critical compressive strain at rupture, $\epsilon_z^* = \Delta z^*/z_0$, versus the Bond number, $Bo = \rho g R_0^2/\sigma$. The data indicates that rupture does not depend on initial radius or liquid surface tension.

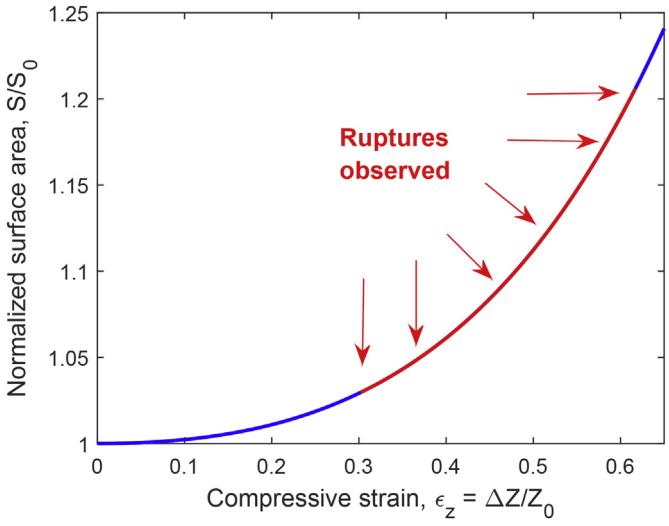

Fig. 10. Normalized surface area, S/S_0, calculated from Eq. (4) versus compressive strain, ϵ_z. The red portion of the curve indicates where ruptures were observed in this study.

Notice that the cracks are typically 1 mm long and hundreds of micrometers wide. In other words, they are always large compared to the particles used in this study. Again, this would imply that the rupture should be independent of the particle size. Indeed, Figs. 8(c) and (d) indicate this is case, i.e. robustness does not depend on particle size. The mean compressive strain at rupture is $\epsilon_z^* \approx 0.49$ whilst the mean elongation strain is $\epsilon_x^* \approx 0.46$, meaning that on average a marble can be crushed down to half of its original height before losing integrity. However, the total range of compressive strain values is from 0.3 up to 0.61 with no quantifiable trend between the data sets. Furthermore, the rupture is also independent of the droplet size and surface tension, best characterized by the Bond number, $Bo = \rho g R_0^2/\sigma$, as indicated by Fig. 9.

The fact that rupture appears to be independent of the liquid properties and powder characteristics thus suggests that the only factor that can determine rupture is the increase in surface area and corresponding decrease in surface coverage. We denote the change in surface area as $\Delta S = S^* - S_0$, where $S_0 \approx 4\pi R_0^2$ is the initial surface area for an approximately spherical marble and S^* is the surface area of the compressed shape just before rupture, which we can take from the pancake model [30] to be

$$S^* \approx 4\pi b^2 + 2\pi^2 ab + 2\pi a^2 \tag{4}$$

where a and b can be found from Eq. (3). Performing this calculation and normalizing with respect to S_0, we can plot the solution against the compressive strain, as shown in Fig. 10.

From this, we see that compressive strains of 30–60% lead to an increase of surface area of about 3–21%. As such, since all the marbles initially appear to be fully coated with particles, if we assume an initial

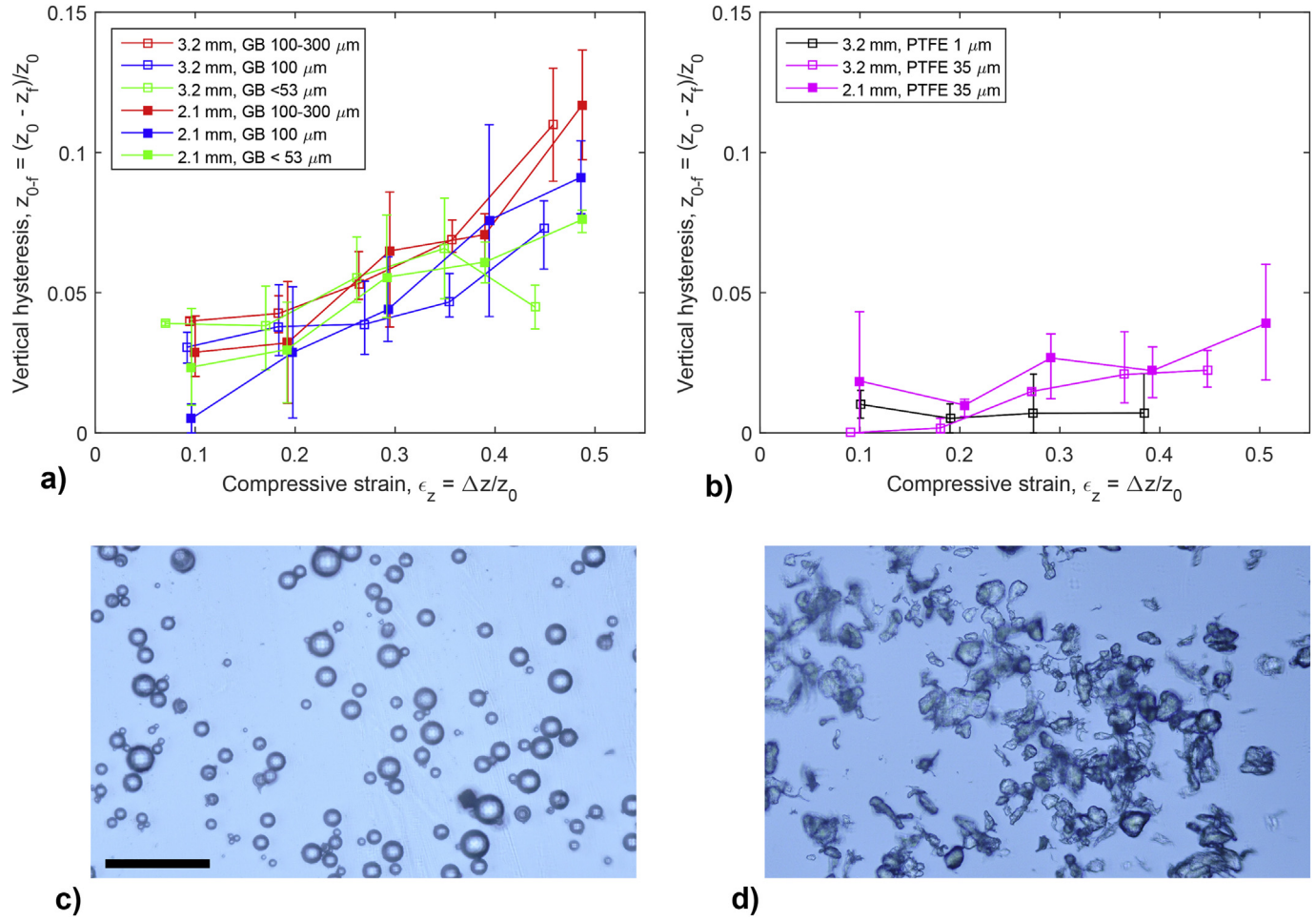

Fig. 11. Hysteresis versus compressive strain for water marbles with (a) glass beads and (b) PTFE powder. Open symbols correspond to marbles with mean initial diameters $D_0 = 3.2$ mm, whilst filled sybols correspond to $D_0 = 2.1$ mm. Particle sizes are given in the legends. Representative microscope images of the two particulates are given in (c) for GB < 53 μm, and (d) for PTFE 35 μm. The scale bar in (c) is 200 μm and applies to both images.

coverage $\Gamma_0 \gtrsim 0.9$ (see refs [23, 35]), and the corresponding particle coverage at rupture, Γ^* is given by:

$$\Gamma^* = \Gamma_0 \frac{S_0}{S^*} \tag{5}$$

then a conservative estimate for the corresponding particle coverage at rupture, is $\Gamma^* \lesssim 0.87 - 0.74$. Again the values of Γ^* do not appear to correlate with particle size or fluid properties.

For large particles, the shell appears to be a monolayer, but there is still some heterogeneity in the packing. For the smaller particles, the initial packing on the surface is very difficult to control due to inter-particle cohesive forces (see for example Fig. 7(a)). Even for nano-particles, the results of [26] indicate that for millimetric marbles, the force at rupture could vary by at least half an order of magnitude between trials. The rupture therefore exhibits an inherent variation which is due to a confluence of heterogenity in the initial packing and distribution of particles sizes, both of which are not easily eliminated.

One final note on the rupture is that the ellipsoid approximation, first introduced by [3], was assumed by [28] but does not accurately describe the shape. It is therefore likely that the surface areas at rupture stated by [28] are overestimates, and by implication the values of ϕ_c in their paper (i.e. the relative surface coverage) are actually underestimates.

3.4. Hysteresis

As described in §3.1, by compressing the marble and then releasing the plate, we can observe hysteresis or an irreversible shape change whereby the marble does not regain its original shape. To study this feature in more detail, we compressed marbles to a prescribed value (before the rupture point) in approximate increments of 10% e.g. $\epsilon_z \approx 0.1$, 0.2, 0.3, etc., at a slow speed $dz/dt = -0.1$ mm/s and then released at the same speed until the top plate was no longer in contact with the marble. The principle measurement is the change in height, $z_0 - z_f$, which we normalize to give the hysteresis as $z_{0-f} = (z_0 - z_f)/z_0$. The results for water marbles are shown in Fig. 11 for (a) glass beads and (b) PTFE powder, which we segregate for clarity.

Fig. 11(a) indicates that the hysteresis is largely a monotonic function of the strain, with the exception of one data point ($D_0 = 3.2$ mm, $d_p < 53$ μm GB, $\epsilon_z = 0.44$), which we assume to be an outlier. Looking at the general trend, we find the hysteresis is small, $z_{0-f} \lesssim 4\%$, for low strains ($\epsilon_z \lesssim 10\%$) but increases gradually up to approximately 10% for the highest strains ($\epsilon_z \approx 50\%$). One interesting observation is that

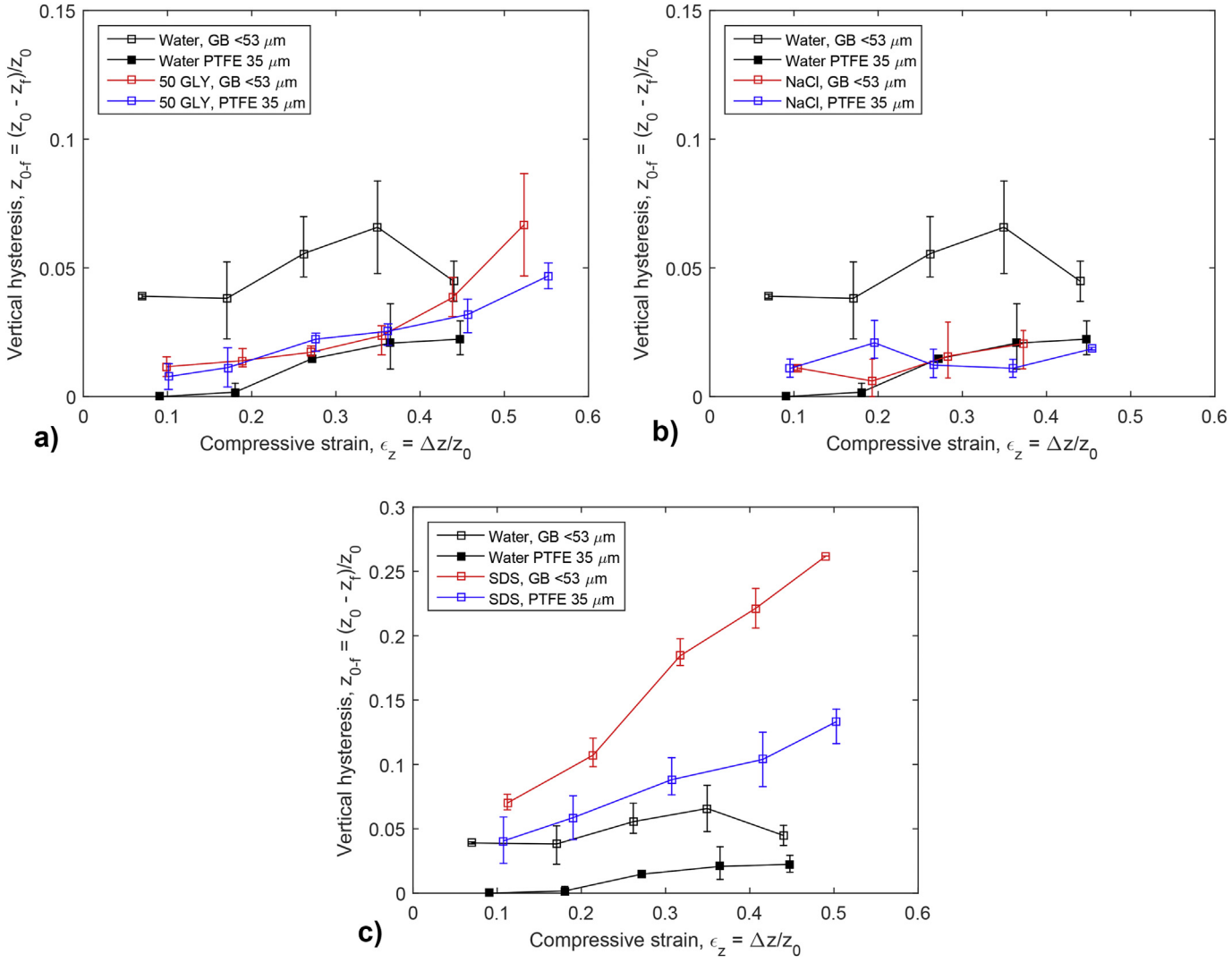

Fig. 12. Hysteresis for different liquids: (a) 50% Glycerin, (b) 29% NaCl, and (c) 3% SDS, for both GB < 53 μm and PTFE 35 μm. The corresponding data for water is replicated in each plot for reference.

there does not appear to be any dependence on particle diameter for low strains, however they de-couple for the highest strains - i.e. the largest hysteresis occurs for the largest particles and the smallest hysteresis occurs for the smallest particles. The data in Fig. 11(b) presents a stark comparison, in that we find the hysteresis to be almost independent of the compressive strain altogether; even for $\epsilon_z = 40$–50%, the hysteresis is only about 1–4%. As such, there is clearly an influence of particle type.

The microscope images in 11 (c) and (d) show that the glass beads are relatively circular and smooth, whilst the PTFE powders are coarse. Previous reports indicate that particle roughness or coarseness leads to a higher degree of particle 'interlocking' (e.g. [38, 39]) but it is unclear how this factor affects the particulate shell during compression. We can only postulate that the relative sphericity of the glass beads permits more structural rearragnement of particles in the polar regions (in contact with the plates) and perhaps more likely to be pushed farther into the interface. This reasoning would also explain the larger hysteresis observed for the larger particles as they can sustain a larger absolute displacement than small particles.

Other than water, Fig. 12 shows that there is a dependence on the underlying composition of the liquid. In particular, we note that the hysteresis is smallest for NaCl marbles ($\sigma = 80$ mN/m), approximately the same as water for the 50% glycerin marbles ($\sigma = 67$ mN/m), but significantly larger for the SDS marbles ($\sigma = 30$ mN/m). Therefore a tentative conclusion is that the hysteresis is inversely correlated with the surface tension of the liquid. We postulate that the large hysteresis for the SDS marbles with glass beads, which can be up to 25%, is due to 'crushing' in the polar regions, which leads to a greater degree of particle impregnation in the liquid surface. This is possible due to the lower contact angles ($\theta \approx 87 - 95^o$) observed with this liquid. As such, particles occupy more of the liquid surface in the curshed regions, which in turn leads to jamming when the compressive stress is removed, as the particles at the splayed edges move back towards the polar regions.

One final point to discuss is that of the effective tension, σ_{eff}, of the marble since it was shown [36] that there can be hysteresis of the effective tension. We are cautious, however, to attribute the hysteresis and irreversibility of shape solely to this factor since the notion of effective tension in the context of liquid marbles is still ambiguous [36, 37] and dependent upon both the experimental configuration *and* the rate of change of surface area. As such, we tentatively conclude that the irreversible change in shape due to compressive strain is a confluence of (i) particle impregnation deeper into the liquid surface, (ii) particle interlocking, and (iii) restructuring in the particle shell, all of which may lead to a change of effective tension.

4. Conclusions

In summary, we have performed an experimental study of the compressive deformation of liquid marbles. The principal result is that under compressive strain, the marble will either rupture or, if released, exhibit shape hysteresis.

As the marble is compressed, the shape is initially spherical with flattened poles, but under higher compression resembles a pancake. The theoretical approximations for these two shapes derived by [30] describe our experimental data well, however the ellipsoid approximation by [3] did not.

At the moment just prior to rupture, when the liquid inside the marble contacts the plates, the shape yields an effective increase in surface area of about 3–21%, which corresponds to a decrease in the surface coverage. The mean surface coverage at rupture was estimated to be $\Gamma_0^* \approx 0.81$, but the range of surface areas at rupture indicate that this can vary considerably.

For trials where the compression was reversed prior to rupture, we observed an irreversible deformation in the shape - i.e. hysteresis, which increased monotonically with compressive strain for glass bead particles, but was very low regardless of strain for the PTFE powders. Regarding the physical origin of the shape hysteresis, it is proposed that particle-shell rearrangement including both particle impregnation into the interface (mainly for large particles) and packing 'densification' (smaller particles) are at play to some extent. To fully understand the origin of the hysteresis, however, future studies looking at particle impregnation and hysteresis after snap-in (e.g. [33]) could be insightful, as well as investigating a range of deformation rates. Furthermore, to fully test the applicability of the shape models of [30], liquid droplets of a variety of diameters and composition should be considered.

References

[1] P. Aussillous, D. Quere, Liquid Marbles, Nature 411 (2001) 924.
[2] D. Quere, P. Aussillous, Non-stick droplets, Chem. Eng. Technol. 25 (2002) 925–928.
[3] Aussillous, P. & Quere, D., Properties of liquid marbles, Proc. R. Soc. A462, 973–999.
[4] C. Zeng, H. Bissig, A.D. Dinsmore, Particles on droplets: from fundamental physics to novel materials, Solid State Commun. 139 (2006) 547–556.
[5] E. Bormashenko, Liquid marbles: properties and applications, Curr. Opin. Colloid Interface Sci. 16 (2011) 266–271.
[6] G. McHale, M.I. Newton, Liquid Marbles: Topical Context Within Soft Matter and Recent Progress, 11, 2015 2530–2546.
[7] M. Dandan, H.Y. Erbil, Evaporation rate of graphite liquid marbles: comparison with water droplets, Langmuir 25 (2009) 8362–8367.
[8] K.P. Hapgood, B. Khanmohammadi, Granulation of hydrophobic powders, Powder Technol. 189 (2009) 253–262.
[9] K.P. Hapgood, L. Farber, J.N. Michaels, Agglomeration of hydrophobic powders via solid spreading nucleation, Powder Technol. 188 (2009) 248–254.
[10] McEleney, P., Walker, G.M., Larmour, I.A. & Bell, S.E.J., Liquid marble formation using hydrophobic powders Chem. Eng. J.147, 373–382.
[11] N. Eshtiaghi, J.J.S. Liu, K.P. Hapgood, Formation of hollow granules from liquid marbles: Small scale experiments, Powder Technol. 197 (2010) 184–195.
[12] J.O. Marston, Y. Zhu, I.U. Vakarelski, S.T. Thoroddsen, Deformed liquid marbles: freezing drop oscillations with powder, Powder Technol. 228 (2012) 424–428.
[13] J.O. Marston, Y. Zhu, I.U. Vakarelski, S.T. Thoroddsen, Freezing drops with powders, Phys. Fluids 25 (2013) 091107.
[14] T. Supakar, M. Moradiafrapoli, G.F. Christopher, J.O. Marston, Spreading, encapsulation and transition to arrested shapes during drop impact onto hydrophobic powders, J. Colloid & Interface Sci. 468 (2016) 10–20.
[15] E. Bormashenko, Liquid marbles, elastic nonstick droplets: from minireactors to self-propulsion, Langmuir 33 (2017) 663–669.
[16] Y. Xue, H. Wang, Y. Zhao, L. Dai, L. Feng, X. Wang, T. Lin, Magnetic liquid marbles: a "precise" miniature reactor, Adv. Mater. 22 (2010) 4814–4818.
[17] J. Tian, T. Arbatan, W. Shen, Liquid marble for gas sensing, Chem. Commun. 46 (2010) 4734–4736.
[18] S. Fujii, M. Suzaki, S. Armes, D. Dupin, S. Hamasaki, K. Aono, Y. Nakamura, Liquid marbles prepared from pH-responsive sterically stabilized Latex particles, Langmuir 27 (2011) 8067–8074.
[19] Y.E. Miao, H.K. Lee, W.S. Chew, I.Y. Phang, T. Liu, X.Y. Ling, Catalytic liquid marbles: Ag nanowire-based miniature reactors for highly efficient degradation of methylene blue, Chem. Commun. 50 (2014) 5923–5926.
[20] Y. Sheng, G. Sun, J. Wu, G. Ma, T. Ngai, Silica-based liquid marbles as microreactors for the silver mirror reaction, Angew. Chem. 54 (2015) 7012–7017.
[21] T. Arbatan, L. Li, J. Tian, W. Shen, Liquid marbles as micro-bioreactors for rapid blood typing, Adv. Healtcare Mat. 1 (2012) 80–83.
[22] Y. Chu, Z. Wang, Q. Pan, Constructing robust liquid marbles for miniaturized synthesis of graphene/ag nanocomposite, Appl. Mater. & Interfaces 6 (2014) 8378–8386.
[23] T. Supakar, A. Kumar, J.O. Marston, Impact dynamics of particle-coated droplets, Phys. Rev. E 95 (2017) 013106.
[24] M. Cui, T. Emrick, T.P. Russell, Stabilizing liquid drops in nonequilibrium shapes by interfacial jamming of nanoparticles, Science 342 (2013) 460–463.
[25] X. Li, Y. Xue, P. Lv, H. Lin, F. Du, Y. Hu, J. Shen, H. Duan, Liquid plasticine: controlled deformation and recovery of droplets with interfacial nanoparticle jamming, Soft Matter 12 (2016) 1655–1662.
[26] P.S. Bhosale, M.V. Panchagnula, H.A. Stretz, Mechanically robust nanoparticle stabilized transparent liquid marbles, Appl. Phys. Lett. 93 (2008) 034109.
[27] S. Asare-Asher, J.N. Connor, R. Sedev, Elasticity of liquid marbles, J.Colloid & Interface Sci. 449 (2015) 341–346.
[28] Z. Liu, X. Fu, B.P. Binks, H.C. Shum, Mechanical compression to characterize the robustness of liquid marbles, Langmuir 31 (2015) 11236–11242.
[29] E. Bormashenko, R. Pogreb, R. Balter, H. Aharoni, Y. Bormashenko, R. Grynyov, L. Mashkevych, D. Aurbach, O. Gendelman, Elastic properties of liquid marbles, Colloid Polym. Sci. 293 (2015) 2157–2164.
[30] G. Whyman, E. Bormashenko, Interpretation of elasticity of liquid marbles, J. Colloid & Interface Sci. 457 (2015) 148–152.

[31] E. Bormashenko, G. Whyman, O. Gendelman, Elastic properties of liquid surfaces coated with colloidal particles, Adv. Condensed Matt. Phys. (2015) 206578.
[32] J.O. Marston, S.T. Thoroddsen, Laser-induced micro-jetting from armored droplets, Exp. Fluids 56 (2015) 140.
[33] C. Li, J.A. Simmons, M. Moradiafapoli, J.O. Marston, Direct visualization of particle attachment to a pendant drop, Soft Matter 13 (2017) 1444–1454.
[34] J.C. Bird, S. Mandre, H.A. Stone, et al., Phys. Rev. Lett. 100 (2008) 234501.
[35] C. Planchette, A.L. Biance, E. Lorenceau, Transition of liquid marble imapcts onto solid surfaces, Euro Phys. Lett. 97 (2012) 14003.
[36] E. Bormashenko, A. Musin, G. Whyman, Z. Barkay, A. Starostin, V. Valtsifer, V. Strelnikov, Revisiting the surface tension of liquid marbles: measurement of the effective surface tension of liquid marbles with the pendant marble method, Colloids & Surfaces A: Physiochem. Eng. 425 (2013) 15–23.
[37] T. Arbatan, W. Shen, Measurement of the surface tension of liquid marble, Langmuir 27 (2011) 12923–12929.
[38] J.O. Marston, E.Q. Li, S.T. Thoroddsen, Evolution of fluid-like granular ejectas generated by sphere impact, J. Fluid Mech. 704 (2012) 5–36.
[39] K.R. Housen, K.A. Holsapple, Ejecta from impact craters, Icarus 211 (2011) 856–875.